Molecular dynamics simulation of classical thermosize effects

Nanoscale and Microscale Thermophysical Engineering, 18: 39–53, 2014

ISSN: 1556-7265 print / 1556-7273 online
DOI: 10.1080/15567265.2013.836692

Taylor & Francis
Taylor & Francis Group

MOLECULAR DYNAMICS SIMULATION OF CLASSICAL THERMOSIZE EFFECTS

Gulru Babac[1] and Jason M. Reese[2]

[1]*Institute of Energy, Istanbul Technical University, Istanbul, Turkey*
[2]*School of Engineering, University of Edinburgh, Edinburgh, Scotland, UK*

We present the first molecular dynamics simulations of classical thermosize effects for realistic molecular conditions and flows. The classical thermosize effect is the chemical potential difference induced between two different-sized channels that have different fluid transport processes. It can be generated by applying a temperature gradient within the different-sized domains, and in this article the system investigated is a combination of a microchannel and a nanochannel. Our molecular dynamics results are compared with a theoretical calculation of the induced chemical potential difference, and this yields useful new insight into diffusive transport in nonequilibrium gas flows.

KEY WORDS: gas flow in micro/nano channels, molecular dynamics, rarefied gas dynamics, thermosize effects

INTRODUCTION

Gas transport in micro- and nanogeometries has attracted a great deal of attention in recent years; see, for example, Goddard et al. [1], Cercignani [2], Karnniadikis et al. [3], and Shen [4]. In a micro- or nanosystem, the mean free path of the gas molecules is comparable to the characteristic size of the domain, and this changes the flow behavior of the gas quite considerably: effects such as the Knudsen process [5–13], thermal creep [14–19], quantum size effects [20–27], and classical thermosize effects (CTSE) [28–30] become important. For example, CTSE arise due to the different flow characteristics of gases subject to a temperature gradient in different-size domains that are connected to each other. The different fluid transport characteristics induce a chemical potential difference between the domains, and this has been analyzed theoretically in the literature by considering a combined macro/nanosystem [28]. In the macrochannel, molecule–molecule collisions dominate and the transport process is conventional hydrodynamics. On the other hand, the transport process in the nanochannel is free molecular flow, and molecule–wall collisions dominate. Therefore, two very different transport processes are coupled when the macro- and nanochannels are connected. This combination of channel sizes produces a very distinct difference between the fluid transport processes, and therefore creates the maximum chemical potential difference.

Manuscript received 18 January 2013; accepted 14 August 2013.

Address correspondence to Gulru Babac, Institute of Energy, Istanbul Technical University, Istanbul 34469, Turkey. E-mail: babac@itu.edu.tr

Color versions of one or more of the figures in the article can be found online at www.tandfonline.com/umte.

NOMENCLATURE

C	constant, m^{-3} $K^{-3/2}$
h	Planck's constant, m^2 kg s^{-1}
Kn	Knudsen number
k_b	Boltzmann constant, m^2 kg s^{-2} K^{-1}
L	characteristic length of the domain, m
l	mean free path of the particles, m
N	number of particles
n	molecule number density, m^{-3}
m	particle mass, kg
p	gas pressure, Pa
R_{ij}	distance between molecules i and j
r_{cut}	cutoff distance in Lennard-Jones potential, m
T	temperature, K
$U(r)$	interaction potential between the molecules

Greek Letters

γ	coefficient
δ	rarefaction parameter
ε	potential depth in Lennard-Jones potential, J
μ	chemical potential for a monatomic ideal gas, J
ρ	mass density, kg/m^3
σ	distance of zero intermolecular potential in Lennard-Jones potential, m
τ	temperature ratio
τ_{T}	coupling parameter in Berendsen thermostat

Subscripts

H	high temperature
L	low temperature
m	macro
n	nano

However, CTSE can also be investigated for other combinations of fluid transport processes if we vary the characteristic length scales of the coupled domains; for example, hydrodynamic with slip-flow processes in macro/micro connected channels or slip flow with continuum-transition processes in connected micro/nanochannels, etc., depending on the operating pressures. The main criterion to observe CTSE is a difference between the transport processes; any system combination that has a difference in the gas flow characteristics can be suitable for CTSE.

In this article, we present a molecular dynamics (MD) simulation of CTSE in a system that combines a microchannel with a nanochannel subject to a temperature gradient. This combination of channel dimensions has been chosen to make the computationally intensive molecular simulations practical in reasonable timescales on a high-performance computer. Both channels are filled with monatomic Maxwellian gases, and the rarefaction conditions are different in each channel because of the difference in channel dimensions. First, the channels are analyzed separately: the density, pressure, and temperature evolutions in the channels are measured and compared with kinetic theory results from the literature. Then the channels are connected to each other and the whole system is investigated for CTSE, and the evolution of the chemical potential is monitored. Our simulation results are compared with available theoretical predictions [28].

CLASSICAL THERMOSIZE EFFECTS

CTSE has been previously studied for monatomic helium gas by considering a rectangular box divided into macro and nano parts [28]. A schematic of this setup is shown in

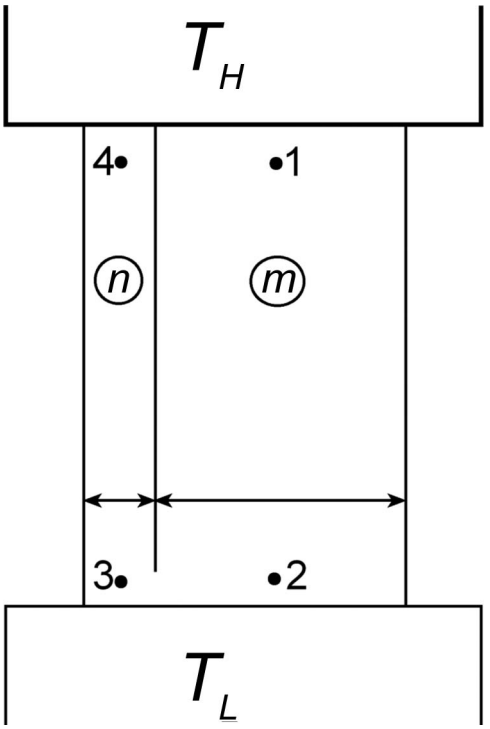

Figure 1 Schematic of the flow system designed to investigate CTSE. Here, *m* indicates the macro section and *n* indicates the nano section.

Figure 1. The separate macro and nano parts are thermally in contact with high-temperature (T_H) and low-temperature (T_L) reservoirs. At the low-temperature end, there is a gap in the separator, and gas flow is allowed between point 2 and point 3 in Figure 1, whereas there is no fluid exchange at the high-temperature end (i.e., between points 1 and 4). Under these conditions, there are different transport processes occurring in each region under the same temperature gradient: the flow characteristics are hydrodynamic and free-molecular in the macro and nano parts, respectively. At steady state, constant thermodynamic properties in each section can be defined through $\nabla p = 0$ in the macro part and $\nabla\left(p/\sqrt{T}\right) = 0$ in the nano part [28], where p is the gas pressure.

These different fluid transport regimes cause different chemical potential gradients under the same temperature gradient. The chemical potential μ for a monatomic ideal gas is

$$\mu = -k_b T \ln\left(\frac{CT^{3/2}}{n}\right), \tag{1}$$

where T is the temperature, k_b is the Boltzmann constant, n is the molecule number density, C is a constant given by $C = (2\pi m k_b)^{3/2}/h^3$, m is the molecular mass, and h is Planck's constant. With the macro and nano parts connected to each other at the low-temperature side, local thermodynamic equilibrium arises in this region, so that $\mu_2 = \mu_3$, $n_2 = n_3$, $T_2 = T_3 = T_L$. The induced chemical potential can also be calculated at the hot temperature

side. So the net chemical potential difference at the hot side, $\Delta\mu = \mu_4 - \mu_1$, has been calculated previously as [28]

$$\Delta\mu = \mu_4 - \mu_1 = \int_{T_L}^{T_H} \left(\frac{\mu_n - \mu_m}{T} \right) dT + \frac{k_b}{2} (T_H - T_L) = -\frac{k_b}{2} T_H \ln(\tau), \tag{2}$$

where the temperature ratio $\tau = T_L / T_H$. This induced chemical potential difference has been termed the CTSE [28]; the name arose because of the strong analogy between this phenomenon and the thermoelectric effect. In the latter, two different kinds of conductors or semiconductors induce an electrochemical potential between them under an applied temperature difference. This is not the case if the materials are the same: different electrical properties of the materials, as well as a temperature gradient, are necessary to observe thermoelectric effects. In the same way, CTSE do not arise if there is no difference in the transport processes between the domains or if there is no temperature gradient applied [28–30].

The induced chemical potential in CTSE could drive a gas flow if, for example, the channels were also connected together at the hot end in Figure 1. In that case, a gas circulation would be started between the domains, producing work. These kinds of circulations have been considered in the literature as a thermodynamic gas cycle [28, 29].

In this article we study CTSE in a micro/nano system using computational molecular dynamics. We model monatomic helium gas, which was also investigated in Babac and Sisman [28, 29]. Though helium gas can be taken as an ideal gas—and this was assumed in these previous papers—it should properly be treated as a real gas in order to be consistent with the MD methodology and its realistic simulation of intermolecular interactions. The chemical potential difference in CTSE also features gases with nonideal character (real gases), and it is calculated theoretically below by using the thermodynamic properties of real gases [31, 32]. Though this is for helium gas, further comparisons with ideal and nonideal gases require many more simulations for different gases that are beyond the scope of the present article.

The chemical potential in Eq. (1) can be modified for nonideal gases to

$$\mu = -k_b T \ln\left(\frac{C T^{3/2} (1 - n\, b(T))}{n} \right) + \frac{n k_b T\, b(T)}{(1 - n b(T))}, \tag{3}$$

where $b(T)$ is the temperature-dependent virial coefficient, which is calculated from the interaction pair potential $U(r)$ between molecules through

$$b(T) = 2\pi \int_0^\infty \left(1 - e^{\left(\frac{U(r)}{k_b T} \right)} \right) r^2 dr. \tag{4}$$

In our simulations we use the common Lennard-Jones (LJ) pair potential, viz.

$$U_{LJ} = 4\varepsilon \left[\left(\frac{\sigma}{R_{ij}} \right)^{12} - \left(\frac{\sigma}{R_{ij}} \right)^{6} \right], \tag{5}$$

and the parameters ε, σ, and R_{ij} are defined in the following section. The net chemical potentials for real gases can then be calculated from Eqs. (3)–(5); that is,

$$\Delta\mu = \mu_4 - \mu_1 = -k_b T_H \ln\left[\frac{n_1}{n_4}\left(\frac{1-n_4 b(T)}{1-n_1 b(T)}\right)\right] + \left(\frac{n_4 k_b T_H\, b(T)}{(1-n_4 b(T))} - \frac{n_1 k_b T_H\, b(T)}{(1-n_1 b(T))}\right) b(T). \tag{6}$$

MOLECULAR DYNAMICS SIMULATIONS

The flow system is investigated using the MD capabilities available in the open-source toolbox OpenFOAM [33–35]. The main purpose of our simulations is to calculate the induced chemical potential difference at the hot end of the channels and compare this with the theoretical results in Babac and Sisman [28] and from Eq. (6).

A monatomic helium gas is considered; the micro and nano channels are thermally in contact with the high-temperature (T_H) and the low-temperature (T_L) reservoirs, and connected to each other at the low-temperature end, as illustrated in Figure 2. Berendsen thermostats with the coupling parameter $\tau_T = 1$ ps are applied [3, 36]; in this way, the reservoir temperatures are kept constant ($T_H = 572.4 \pm 0.014$ K and $T_L = 286.2 \pm 0.015$ K) and the necessary temperature gradient is developed. Boundary conditions (BCs) are set as diffusive wall, and diffusive wall with a linear temperature gradient, along the y- and x-directions, respectively. In the z-direction, periodic BCs are applied. Applying wall BCs with a linear temperature gradient has the advantage that heat is transferred from the wall to the fluid, and this provides a more accurate representation of the system: when a gas molecule passes this boundary it is reinserted back into the simulation domain with a velocity sampled from an equilibrium Maxwell-Boltzmann distribution at the local temperature of the wall.

As stated above, the helium atoms interact with each other through an LJ potential. For helium–helium interactions we used the LJ values $\varepsilon_{He-He} = 1.9654 \times 10^{-22}$ J and $\sigma_{He-He} = 2.2023 \times 10^{-10}$ m [37]. The potential is truncated and shifted at a distance $r_{\text{cut}} = 6.6 \times 10^{-10}$ m in order to improve the computational speed of the MD simulations, without affecting the accuracy significantly. A time step of 1.28 fs is used. Each part of the system is initialized with the same density, $\rho = 0.0685$ kg/m^3. Defining the Knudsen

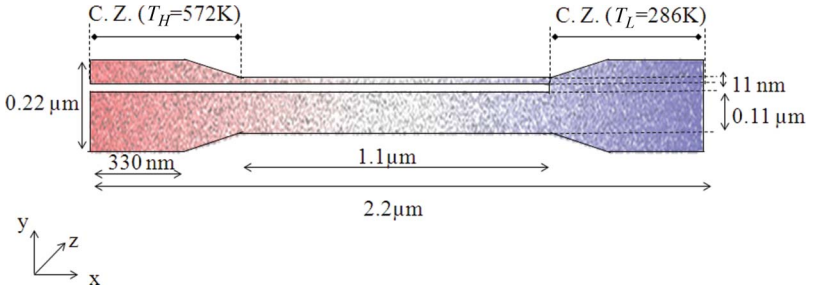

Figure 2 Schematic of the simulated MD system. The channel depth is a uniform 22 nm throughout the system. Here, the helium atoms are colored according to temperature: red denotes high temperature and blue denotes low temperature. Berendsen thermostats are applied within the control zones (C.Z.) to maintain the temperatures labeled, and the wall boundary conditions are diffusive.

number Kn as the ratio of the mean free path of the molecules $\left(l = 1\Big/\sqrt{2}\pi\sigma^2 n\right)$ to the characteristic length L of the domain (chosen here as the respective channel width), the rarefaction parameter $\delta = \sqrt{\pi}\Big/(2\,Kn)$ is 0.0177 in the nanochannel and 0.177 in the microchannel.

The gas pressure in the MD simulations is calculated by

$$p = \frac{1}{V}\sum_{i}^{N}\left(m_i u_i^2 + \frac{1}{3}\sum_{j>1}^{N} F\left(R_{ij}\right) R_{ij}\right) + \frac{16}{3}\pi\rho^2\left[\frac{2}{3}\left(\frac{1}{r_{\text{cut}}}\right)^9 - \left(\frac{1}{r_{\text{cut}}}\right)^3\right], \tag{7}$$

where m is the molecular mass, u is the molecular velocity, V is the system volume, ρ is the density of the gas, and $F(R_{ij})$ is the intermolecular force between two interacting molecules a distance R_{ij} apart. Equation (7) includes the standard kinetic and virial terms for the pressure calculation and also the tail correction when LJ interactions are involved, as in our case [38].

In all of the simulations we present here, the uncertainty in calculated fluid properties does not exceed 2% over the whole domain. The oscillations in the pressure and density values at steady state are ± 0.1 kPa and $\pm 0.0019\ \text{kg/m}^3$, respectively, with the uncertainty in the calculations between 0.9 and 1.1%. In the nanochannel, the uncertainty in the pressure value is a maximum of 1.98%, with oscillations of ± 0.3 kPa.

The definition of constant processes in the channels will also be useful for our calculations. A zero net flux condition in the free molecular regime has the following relation between the pressure and temperature [39]:

$$\frac{1}{p}\frac{\partial p}{\partial x} = \frac{\gamma}{T}\frac{\partial T}{\partial x}. \tag{8}$$

For the low- and high-temperature ends, these can be related through

$$\frac{p_H}{p_L} = \left(\frac{T_H}{T_L}\right)^{\gamma}, \tag{9}$$

which can be rewritten as $p_H\big/T_H^{\gamma} = p_L\big/T_L^{\gamma}$ with $p\big/T^{\gamma}$ representing the constant process in the domain. Through the product rule $(\nabla(fg) = f\,\nabla g + g\,\nabla f \;\Rightarrow\; \nabla(pT^{-\gamma}) = p\,\nabla(T^{-\gamma}) + T^{-\gamma}\,\nabla p)$, this process can be also written in the following form:

$$\nabla\left(p/T^{\gamma}\right) = 0. \tag{10}$$

Using the ideal gas law $p = nk_bT$, this equation can also be written in terms of the number density:

$$\frac{n_H}{n_L} = \left(\frac{T_H}{T_L}\right)^{\gamma-1}, \tag{11}$$

or, in gradient form,

$$\nabla\left(nT^{1-\gamma}\right) = 0. \tag{12}$$

In Eqs. (9) and (11), γ is a function of the rarefaction parameter and can be determined analytically depending on the geometry, nature of the molecular interactions, type of gas, etc. [40]. The familiar Knudsen equation can be obtained from Eq. (9) in the free-molecular limit by setting $\gamma = 0.5$.

In our molecular simulations, initially both channels are simulated separately, and pressure, temperature, and density measurements are made at the steady state. Simulations are run for the channels without any connection domain between them; γ for each separate channel is calculated and compared with the kinetic theory result [40]. Then the two separate channels are connected via the additional domain at the low-temperature side, so gas flow between the channels is allowed and thermodynamic equilibrium is achieved in the connection domain at the low-temperature end. This then replicates the system reported in Babac and Sisman [28].

RESULTS AND DISCUSSION

The simulated temperature, pressure, and density profiles along each separate channel are presented in Figures 3 and 4. Inlet/outlet effects can be seen at the hot end (at $\sim$0.55 μm) and cold end (at $\sim$1.65 μm) of the channels as pressure, density, and temperature jumps. These jumps are slightly higher in the nanochannel because of the lower rarefaction parameter, but they decrease with increasing rarefaction parameter; in the continuum limit, they disappear and the profiles become smoother [41].

Using Eq. (9) or (11), γ is calculated from the pressure and temperature measurements and given in Table 1, alongside the kinetic theory results from Sharipov [40]. Our MD results for the microchannel (for $\delta = 0.177$) are consistent with the theoretical ones. The small difference between the values can be attributed to using an LJ intermolecular potential and from the pressure calculation.

For the nanochannel ($\delta = 0.0177$), γ is higher than the theoretical prediction. In free-molecular flow (or close to free-molecular flow) some discrepancies between theory, experiments, and simulations have also appeared in the literature [19, 41]. These discrepancies could be caused by "end effects," which are not taken into account in the kinetic theory, and these can dominate in the free molecular regime and in systems that have low length-to-height ratios. This would especially affect pressure calculations in highly rarefied gases, because the pressure losses at the inlet and outlet of the channel are higher for higher rarefaction. Measurements of pressure in highly rarefied gases are in any case difficult using MD: intermolecular interactions in the pressure calculations can involve further correction terms. The discrepancy in free-molecular flow results could also be due to Knudsen layer effects close to solid surfaces [42].

The high temperature difference imposed on the system could also be the reason for the observed difference in γ. In kinetic theory it is generally assumed that variations in temperature are very small [40]. However, a small temperature difference is not suitable for modeling CTSE: as the temperature difference decreases toward zero, CTSE vanishes. For this reason, we applied a temperature ratio of 2:1 from end to end of our simulated system and $\Delta T \cong 286$.

Under these conditions, any overpredicted γ value may still be acceptable, because CTSE depends on the density gradient along the channel and an overpredicted γ corresponds to an underpredicted density difference, as can be seen from Eq. (11). Therefore, the magnitude of the CTSE we observe may be less than it would be in a real experiment.

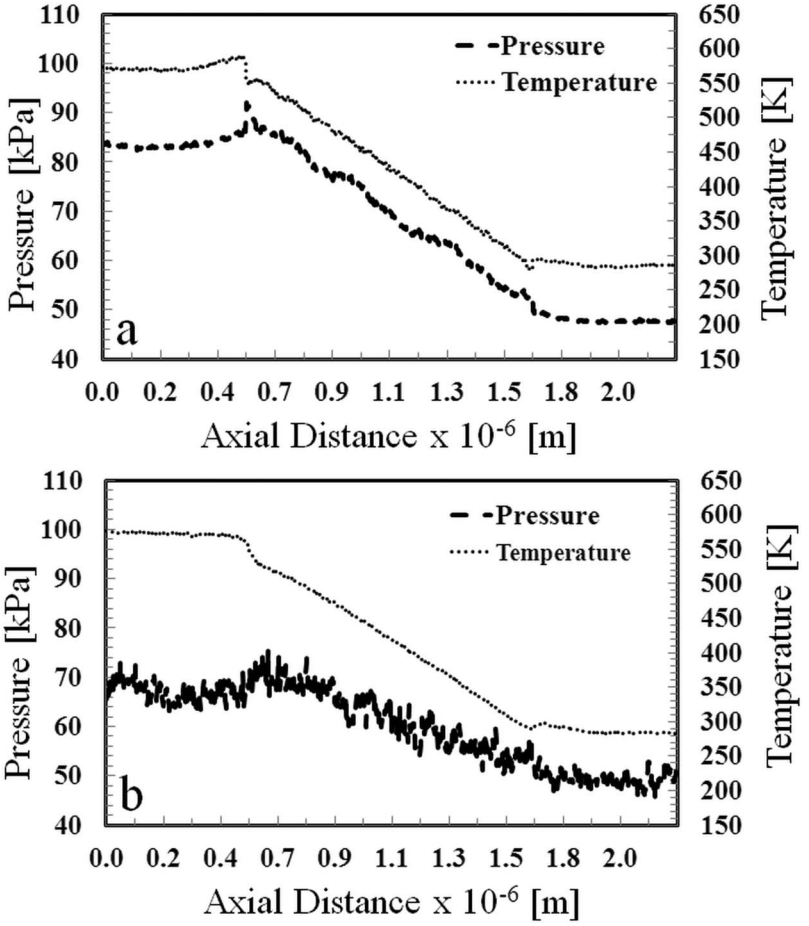

Figure 3 Simulated pressure and temperature profiles along the centerline of the separate (a) nanochannel and (b) microchannel.

This would therefore not change our conclusions about the existence of CTSE, which are discussed below.

After these initial simulations, the two separate channels are connected through an additional domain at the low-temperature end, and the MD simulation is run again to steady state. The pressure and temperature profiles for the nano- and microcomponents of the full system are presented in Figure 5. As seen in this figure, the data are fluctuating more in the nanochannel than in the microchannel. This is due to the number of molecules in the channels: both channels are initialized with the same density value, which corresponds to fewer molecules in the nanochannel than in the microchannel. The fluctuation in MD data is proportional to $1/\sqrt{N}$, with N the number of molecules. In this case, the number of molecules in the nanochannel is 15,930, and there are 67,050 in the microchannel. The error due to pressure fluctuations is 1.98% in the nanochannel and less than 1% in the microchannel.

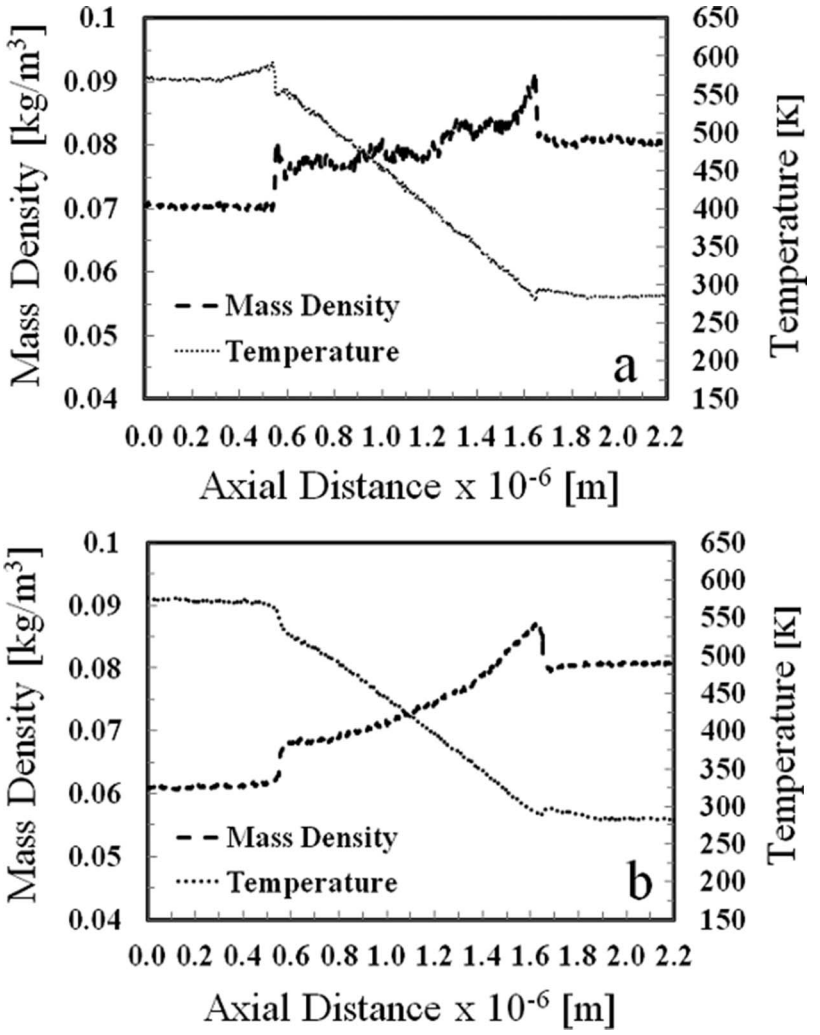

Figure 4 Simulated density and temperature profiles along the centerline of the separate (a) nanochannel and (b) microchannel.

Table 1 γ values for the micro- and nanochannels

	γ values for purely diffusive reflection	
Rarefaction parameter, δ	MD simulation result	Kinetic theory result [40]
0.177	0.4288	0.4337
0.0177	0.6665	0.4873

The rarefaction parameter δ in both parts of the combined system is calculated and presented in Table 2. Comparing the results in Tables 1 and 2, the γ value for the microchannel in the combined system increases, whereas it decreases for the nanochannel. This is understandable in terms of the density variation in the channels: at the same temperature

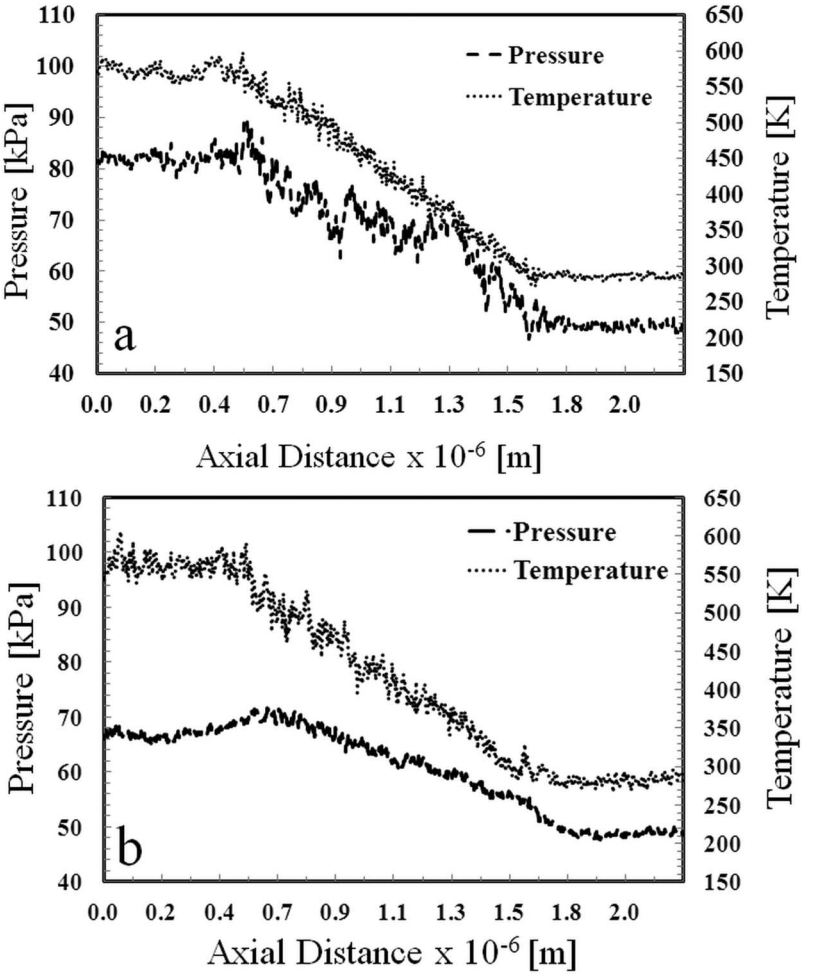

Figure 5 Simulated pressure and temperature profiles in the combined system: (a) nanochannel part and (b) microchannel part.

Table 2 γ values for micro- and nanochannel parts of the combined system

	γ values for purely diffusive reflection	
Rarefaction parameter, δ	MD simulation result	Kinetic theory result [40]
0.177	0.4461	0.4337
0.0177	0.6370	0.4873

gradient, the molecular number density in the low-temperature end of the microchannel n_2 is higher than that of the nanochannel n_3 (where n_2 and n_3 represent the densities at point 2 and point 3 in Figure 1, respectively). With $n_2 > n_3$ at the low-temperature end of the channels, molecules tend to move from the micro side to the nano side through the additional domain (i.e., from point 2 to point 3 in Figure 1) as the simulation proceeds to

steady state. This continues until equilibrium ($n_2 = n_3$) is reached at the low-temperature end at steady state. This means there is a slight increase in the number of molecules in the nanochannel and a slight decrease in the number of molecules in the microchannel. This is manifested as a difference in γ between the separate and the combined systems, amounting to 4 and 5% for the micro- and nanochannels, respectively. The rarefaction parameters in Table 2 will also be slightly lower for the nanochannel and higher for the microchannel at steady state.

With the γ values from Table 2 and the constant process in the combined nano- and microchannel system, we have

$$\nabla\left(p/T^{0.6370}\right)_{\text{nano\_channel}} = 0 \tag{13}$$

and

$$\nabla\left(p/T^{0.4461}\right)_{\text{micro\_channel}} = 0. \tag{14}$$

(We note that if the γ values are set to be 0.5 and 1, free-molecular flow and hydrodynamic flow conditions would be obtained, respectively, as discussed above.) In CTSE, this difference in the transport processes is reflected in a chemical potential difference between the channels, and this difference can be calculated at the hot end of the channels. However, these calculations require density values, as seen in Eq. (6), so before calculating the chemical potential calculations it is important to analyze the density variation along the channels.

The density profiles for each of the channels in the combined system are given in Figure 6. As can be seen, the densities at the low-temperature end are equal to each other because of thermodynamic equilibrium. Inlet/outlet effects can be seen at both ends of the channels, as discussed above. The profiles of the densities are different because of the different transport processes in the different channels. This difference along the channels

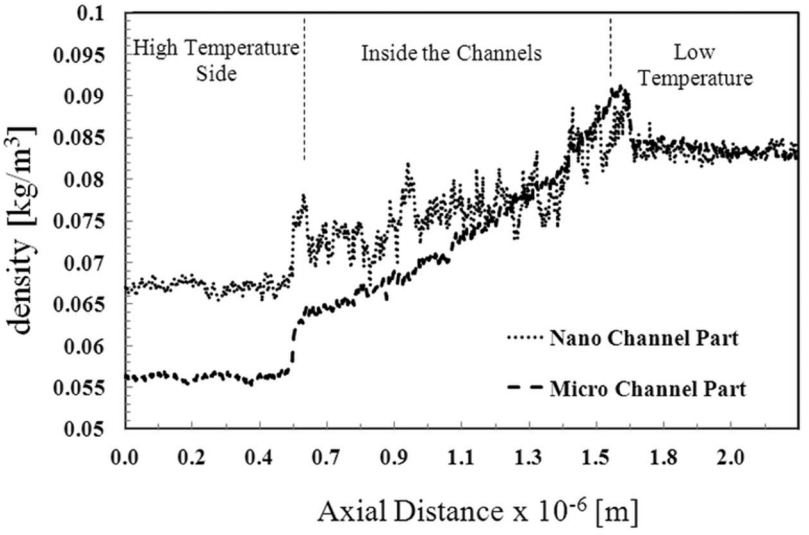

Figure 6 Simulated density distribution in the micro and the nano parts of the combined system.

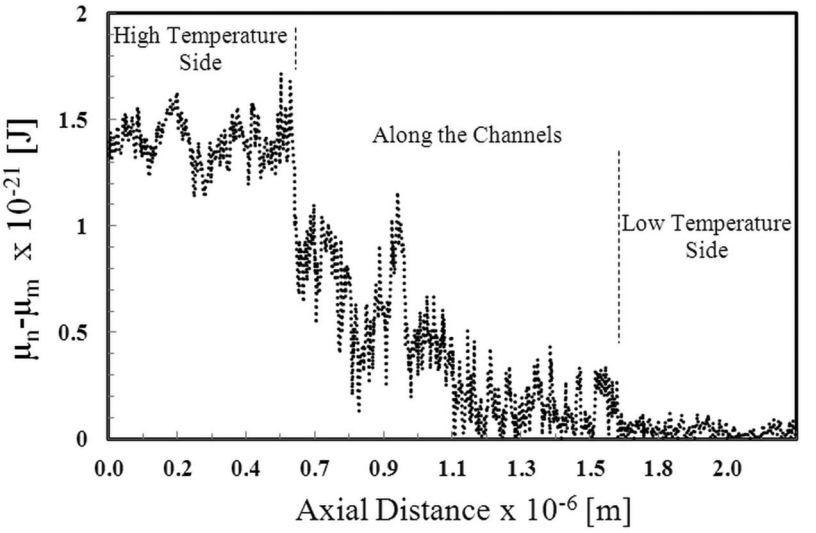

Figure 7 Distribution of the chemical potential difference along the combined system.

induces a chemical potential difference, which is presented in Figure 7. This figure shows that there is no chemical potential difference at the low-temperature end because of the thermodynamic equilibrium conditions. Along the channel, the chemical potential difference varies, with the maximum net difference obtained at the hot temperature end of the system.

The maximum net chemical potential difference, $(\mu_4 - \mu_1)$, can be calculated for nonideal helium gas using Eq. (6) to be 1.5×10^{-21} J, which is the same value that the data fluctuates around in Figure 7. In Babac and Sisman [28], for the ideal gas situation, the maximum potential difference is calculated to be 2.73×10^{-21} J. One reason why this latter value differs from our MD result is that in Babac and Sisman [28] all of the irreversibilities in the system are ignored, whereas MD simulations are more realistic. However, the main reason is the difference in the domain sizes studied; in other words, the differences in the transport processes involved. Babac and Sisman [28] considered a macro/nanosystem in which continuum and free-molecular processes were combined. In our simulations here, there are smaller differences in rarefaction between the two components of the combined micro/nano system, in order for the MD simulations to complete within a reasonable time. Therefore, we expect to see a smaller CTSE effect in our simulations here. Though both theoretical and computational results are of the same order of magnitude, our chemical potential difference is about 45% of the theoretical ideal gas value in Babac and Sisman [28].

CONCLUSIONS

We have demonstrated through numerical molecular experiments the existence of an induced chemical potential difference due to CTSE. This chemical potential difference arises when different transport processes are coupled together under the same temperature gradient. To the best of our knowledge, we have presented the first MD results for a micro/nano combined system that displays CTSE. Because MD simulations are

deterministic and can emulate realistic molecular conditions and flows, this advances understanding about CTSE because the effect has previously only been discussed theoretically in the literature.

The MD-simulated chemical potential difference induced through CTSE has been compared with a previous theoretical analysis. Though there are important geometrical differences between the systems considered theoretically in Babac and Sisman [28] and computationally in this article, the results are of the same order of magnitude, with the MD result somewhat lower, as expected. Though MD simulations of the exact macro- and nanochannel configuration in Babac and Sisman [28] would require extreme computational effort, statistical particle methods, such as the direct simulation Monte Carlo technique, may prove more practical in these circumstances. Further simulations are necessary to build more understanding about how CTSE varies with different temperature gradients, different rarefaction conditions, different geometries of the domains, etc.

The chemical potential difference induced through CTSE can drive a circulating gas flow if the channels are fully connected to each other at both ends. This kind of gas circulation could be exploited for new power and refrigeration cycles in nanoscale systems. Higher temperature gradients and greater differences of rarefaction in the working gas can increase the induced chemical potential difference and the efficiency of any technological system based on CTSE.

ACKNOWLEDGEMENTS

G.B. would like to thank the Scientific and Technological Research Council of Turkey (TUBITAK) for partial funding of this research. OpenFOAM is free to download from www.openfoam.org. JMR would like to thank the UK's EPSRC for funding under grant no. EP/I011927/1.

REFERENCES

1. W.A. Goddard, D.W. Brenner, S.E. Lyshevski, and G.J. Iafrate, *Handbook of Nanoscience, Engineering and Technology*, CRC Press, Boca Raton, FL, 2003.
2. C. Cercignani, Rarefied Gas *Dynamics: From Basic Concepts to Actual Calculations*, Cambridge University Press, Cambridge, UK, 2000.
3. G.E. Karniadikis, N. Aluru, and A. Beskok, Micro and Nano Flows: *Fundamentals and Simulation*, Springer, New York, 2005.
4. G. Shen, *Rarefied Gas Dynamics: Fundamentals Simulations and MicroFlows*, Springer-Verlag, Berlin, 2005.
5. O. Reynolds, On Certain Dimensional Properties of Matter in the Gaseous State, *Philosophical Transactions of the Royal Society of London*, Vol. 170, pp. 727–845, 1880.
6. T. Graham, On the Molecular Mobility of Gases, *Philosophical Transactions of the Royal Society of London*, Vol. 153, pp. 385–405, 1863.
7. M. Knudsen, Eine Revision der Gleichgewichsbedingung der Gase. Thermische Molekularstromung, *Annalen der Physik*, Vol. 336, No. 1, pp. 205–229, 1909.
8. M. Knudsen, Thermischer Molekulardruck der Gase in Rohren, *Annalen der Physik*, Vol. 336, pp. 1435–1448, 1910.
9. A.A. Alexeenko, S.F. Gimelshein, E.P. Muntz, and A.D. Ketsdever, Kinetic Modelling of Temperature Driven Gas Flows in Short Channels, *International Journal of Thermal Sciences*, Vol. 45, pp. 1045–1051, 2006.

10. D. Copic and S. McNamara, Efficiency Derivation for Knudsen Pump with and without Thermal Losses, *Journal of Vacuum Science and Technology*, Vol. 27, pp. 496–502, 2009.
11. S. McNamara and Y.B. Ganhandani, On-Chip Vacuum Generated by a Knudsen Pump, *Journal of Microelectromechanical Systems*, Vol. 14, pp. 741–746, 2005.
12. S. Takata, H. Sugimoto, and S. Kosuge, Gas Separation by Means of the Knudsen Compressor, *European Journal Mechanics B - Fluids*, Vol. 26, pp. 155–181, 2007.
13. S.E. Vargo, E.P. Muntz, G.R. Shiflett, and W.C. Tang, The Knudsen Compressor as a Micro and Macroscale Vacuum Pump without Moving Parts or Fluids, *Journal of Vacuum Science and Technology*, Vol. 17, pp. 2308–2313, 1999.
14. S.K. Loyalka, Thermal Transpiration in a Cylindrical Tube, *Physics of Fluids*, Vol. 12, pp. 2301–2305, 1969.
15. E.H. Kennard, On the Thermodynamics of Thermal Transpiration and of the Thomson Effect, *Physical Review*, Vol. 22, pp. 617–621, 1923.
16. S.K. Loyalka, Kinetic Theory of Thermal Transpiration and Mechanocaloric Effect II, *The Journal of Chemical Physics*, Vol. 63, pp. 4054–4060, 1975.
17. B.K. Annis, Thermal Creep in Gases, *The Journal of Chemical Physics*, Vol. 57, pp. 2898–2905, 1972.
18. H.C. Weng and C. Chen, On the Importance of Thermal Creep in Natural Convective Gas Microflow with Wall Heat Fluxes, *Journal of Physics D: Applied Physics*, Vol. 41, 115501, 2008.
19. Y.L. Han, E.P. Muntz, A. Alexeenko, and M. Young, Experimental and Computational Studies of Temperature Gradient–Driven Molecular Transport in Gas Flows through Nano/Microscale Channels, *Nanoscale and Microscale Thermophysical Engineering*, Vol. 11, pp. 151–175, 2007.
20. A. Sisman and I. Muller, The Casimir-Like Size Effects in Ideal Gases, *Physics Letters A*, Vol. 320, pp. 360–366, 2004.
21. A. Sisman, Surface Dependency in Thermodynamics of Ideal Gases, *Journal of Physics A: Mathematical and General*, Vol. 37, pp. 11353–11361, 2004.
22. A. Sisman, Z.F. Ozturk, and C. Firat, Quantum Boundary Layer: A Non-uniform Density Distribution of an Ideal Gas in Thermodynamic Equilibrium, *Physics Letters A*, Vol. 362, pp. 16–20, 2007.
23. Z.F. Ozturk and A. Sisman, Quantum Size Effects on the Thermal and Potential Conductivities of Ideal Gases, *Physica Scripta*, Vol. 80, 065402, 2009.
24. C. Firat and A. Sisman, A Universality of the Quantum Boundary Layer for a Maxwellian Gas, *Physica Scripta*, Vol. 79, 065002, 2009.
25. W.S. Dai and M. Xie, Quantum Statistics of Ideal Gases in Confined Space, *Physics Letters A*, Vol. 311, pp. 340–346, 2003.
26. W.S. Dai and M. Xie, Geometry Effects in Confined Space, *Physical Review E*, Vol. 70, pp. 1–12, 2004.
27. W. Nie and J. He, Performance Analysis of a Thermosize Micro/Nano Heat Engine, *Physics Letters A*, Vol. 372, pp. 1168–1173, 2008.
28. G. Babac and A. Sisman, Thermodynamic Cycles Based on Classical Thermosize Effects, *Journal of Computational and Theoretical Nanoscience*, Vol. 8, pp. 1720–1726, 2011.
29. G. Babac and A. Sisman, Classical Thermosize Effects in Degenerate Quantum Gases, *Journal of Computational and Theoretical Nanoscience*, Vol. 8, pp. 2331–2334, 2011.
30. A. Sisman and G. Babac, Quantum Size Effects on Classical Thermosize Effects, *Continuum Mechanics and Thermodynamics*, Vol. 24, pp. 339–346, 2012.
31. L.D. Landau and E.M. Lifshitz, *Statistical Physics*: *Part 1: Vol. 5. Course of Theoretical Physics*, Pergamon Press, London, 1958.
32. J.A. Fay, *Molecular Thermodynamics*, Addison-Wesley, Boston, MA, 1965.
33. G.B. Macpherson and J.M. Reese, Molecular Dynamics in Arbitrary Geometries: Parallel Evaluation of Pair Forces, *Molecular Simulation*, Vol. 34, No. 1, pp. 97–115, 2008.
34. G.B. Macpherson, M.K. Borg, and J.M. Reese, Generation of Initial Molecular Dynamics Configurations, *Molecular Simulation*, Vol. 33, pp. 1199–1212, 2007.

35. M.K. Borg, G.B. Macpherson, and J.M. Reese, Controllers for Imposing Continuum-to-Molecular Boundary Conditions in Arbitrary Fluid Flow Geometries, *Molecular Simulation*, Vol. 36, No. 10, pp. 745–757, 2010.
36. P.H. Hünenberger, Thermostat Algorithms for Molecular Dynamics Simulations, *Advances in Polymer Science*, Vol. 173, pp. 105–149, 2005.
37. E.J. Arlemark and J.M. Reese, Investigating the Effect of Solid Boundaries on the Gas Molecular Mean-Free-Path, *Proceedings of the 7th International ASME Conference on Nanochannels, Microchannels and Minichannels*, 22–24 June 2009.
38. D. Frenkel and B. Smit, *Understanding Molecular Simulation: From Algorithms to Applications*, Academic Press, San Diego, CA, 2002.
39. F. Sharipov and V. Seleznev, Data on Internal Rarefied Gas Flow, *Journal of Physical and Chemical Reference Data*, Vol. 27, No. 3, pp. 657–706, 1998.
40. F. Sharipov, Rarefied Gas Flow through a Long Tube at Any Temperature Ratio, *Journal of Vacuum Science & Technology A*, Vol. 14, No. 4, pp. 2627–2635, 1996.
41. G. Babac, N. Dongari, and J.M. Reese, Thermal Transpiration of Nanoscale Gas Flow, *Proceedings of the 28th International Symposium on Rarefied Gas Dynamics*, Vol. 1501, pp. 946–953, 2012.
42. N. Dongari, Y.H. Zhang, and J.M. Reese, Molecular Free Path Distribution in Rarefied Gases, *Journal of Physics D: Applied Physics*, Vol. 44, paper 125502, 2011.